Supplemental for "Quantifying Seasonal and Interannual Variability in Surface Stress and Mixed-Layer Entrainment in the Central Canada Basin"

Elizabeth Bailey[1], Annika Margevich[1], and Mary-Louise Timmermans[1]

[1]Department of Earth and Planetary Sciences, Yale University

Correspondence: Elizabeth Bailey (elizabeth.bailey@yale.edu)

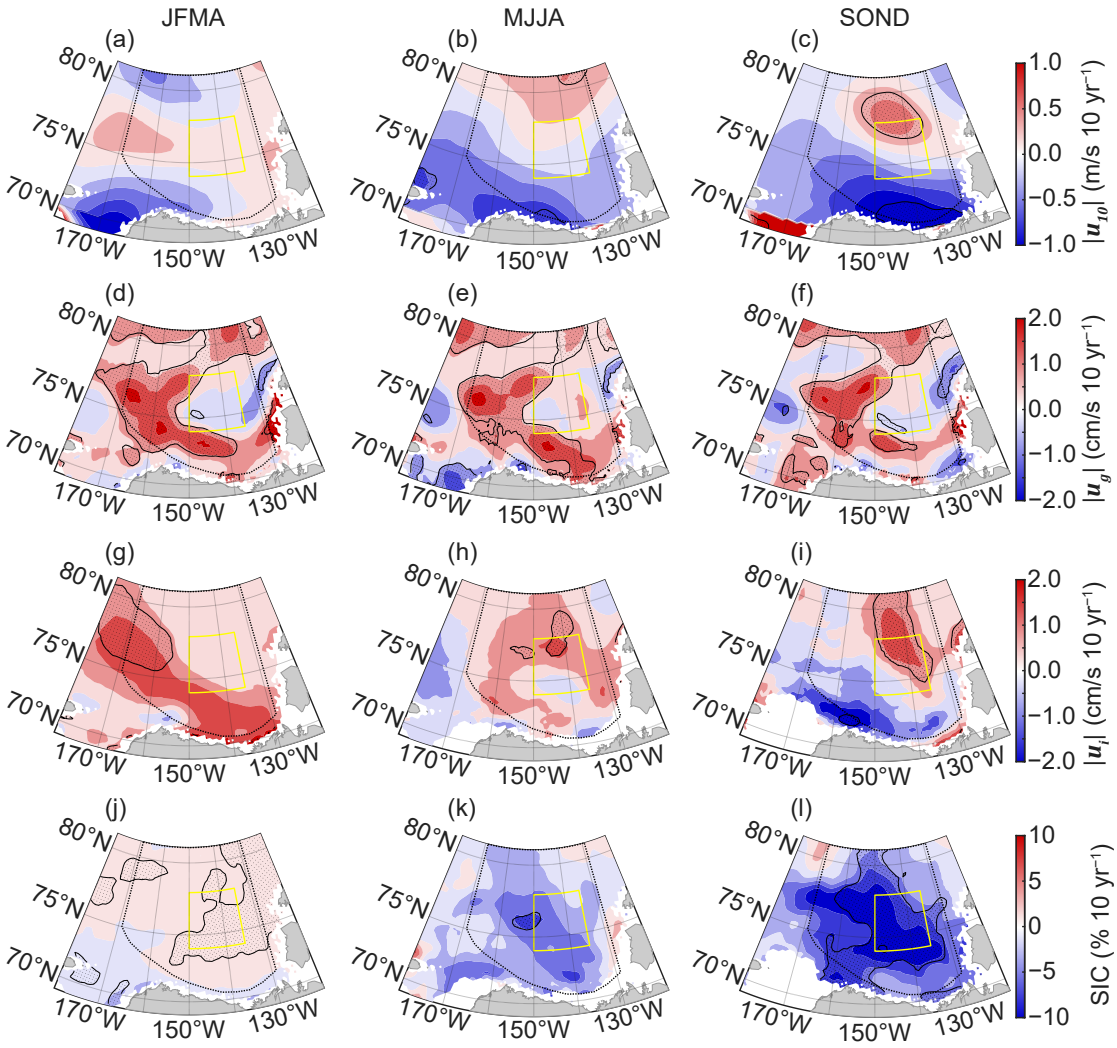

Figure S1. Interannual linear trends in 10 m wind speed ($|\boldsymbol{u_{10}}|$) for the seasonal mean of a) January–April (JFMA), b) May–August (MJJA), and c) September–December (SOND) for 2003–2023. Data from ERA5 Reanalysis. Interannual linear trends in geostrophic current speed ($|\boldsymbol{u_g}|$) for the seasonal mean of d) JFMA, e) MJJA, and f) SOND for 2003–2023. These data are from DOT data (Armitage et al., 2016, 2017; Lin et al., 2023). Interannual linear trends in ice drift speed ($|\boldsymbol{u_i}|$) for the seasonal mean of g) JFMA, h) MJJA, and i) SOND for 2003–2023. Interannual linear trends in SIC for the seasonal mean of j) JFMA, k) MJJA, and l) SOND for 2003–2023. Ice drift velocities are from the Polar Pathfinder Daily 25 km EASE-Grid Sea Ice Motion Vectors, version 4 and SIC is from Nimbus-7 SMMR and DMSP SSM/I-SSMIS Passive Microwave Data Version 2 (Tschudi et al., 2019; DiGirolamo et al., 2022). Dotted regions indicate statistically significant trends at the 95% confidence level. Trends in gridboxes that are ice-free (defined when SIC ≤ 0.15) for more than 5% of the 2003–2023 timeseries are neglected and not shown in the $|\boldsymbol{u_i}|$ and SIC maps.

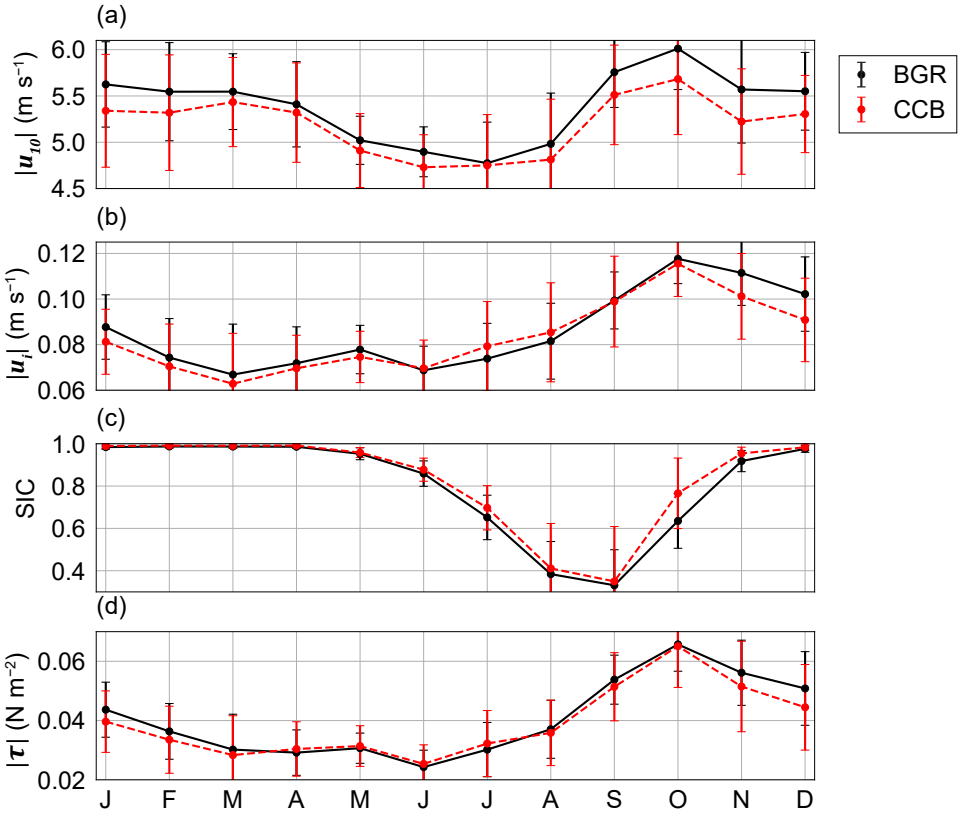

Figure S2. Monthly mean a) 10 m wind speed ($|\boldsymbol{u_{10}}|$), b) sea-ice drift speed ($|\boldsymbol{u_i}|$), c) sea ice concentration (SIC), and d) magnitude of total surface stress ($|\boldsymbol{\tau}|$) over the Beaufort Gyre region (BGR, black) and the central Canada basin (CCB, red) for the 2003–2023 period. Error bars indicate one interannual standard deviation.

References

Armitage, T. W. K., Bacon, S., Ridout, A. L., Thomas, S. F., Aksenov, Y., and Wingham, D. J.: Arctic sea surface height variability and change from satellite radar altimetry and GRACE, 2003–2014, Journal of Geophysical Research: Oceans, 121, 4303–4322, https://doi.org/10.1002/2015JC011579, 2016.

Armitage, T. W. K., Bacon, S., Ridout, A. L., Petty, A. A., Wolbach, S., and Tsamados, M.: Arctic Ocean surface geostrophic circulation 2003–2014, The Cryosphere, 11, 1767–1780, https://doi.org/10.5194/tc-11-1767-2017, 2017.

DiGirolamo, N., Parkinson, C., Cavalieri, D., Gloersen, P., and Zwally, H.: Sea Ice Concentrations from Nimbus-7 SMMR and DMSP SSM/I-SSMIS Passive Microwave Data, Version 2, https://doi.org/10.5067/MPYG15WAA4WX, 2022.

Lin, P., Pickart, R. S., Heorton, H., Tsamados, M., Itoh, M., and Kikuchi, T.: Recent state transition of the Arctic Ocean's Beaufort Gyre, Nature Geoscience, 16, 485–491, https://doi.org/10.1038/s41561-023-01184-5, 2023.

Margevich, A., Timmermans, M.-L., and Danielson, S.: Drivers of Ekman Pumping and Subduction in the Northern Chukchi Sea and Implications for Interior Beaufort Gyre Waters, Submitted to Journal of Geophysical Research: Oceans.

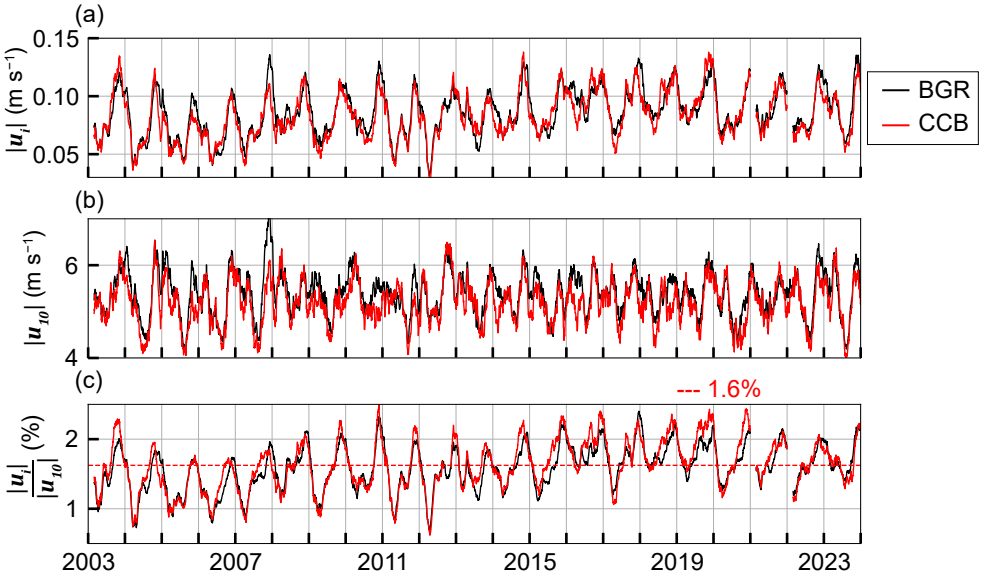

Figure S3. 30-day running mean timeseries of the mean a) ice drift speed ($|\boldsymbol{u_i}|$), b) 10 m wind speed ($|\boldsymbol{u_{10}}|$), and the ratio of ice speed to wind speed as a percentage ($\frac{|\boldsymbol{u_i}|}{|\boldsymbol{u_{10}}|} \times 100$) over the Central Canada Basin (CCB) from 2003–2023. The red horizontal line indicates the 2003–2023 climatological mean wind factor for the CCB (1.6%).

Tschudi, M., Meier, W. N., Stewart, J. S., Fowler, C., and Maslanik, J.: Polar Pathfinder Daily 25 km EASE-Grid Sea Ice Motion Vectors, https://doi.org/10.5067/INAWUWO7QH7B, 2019.

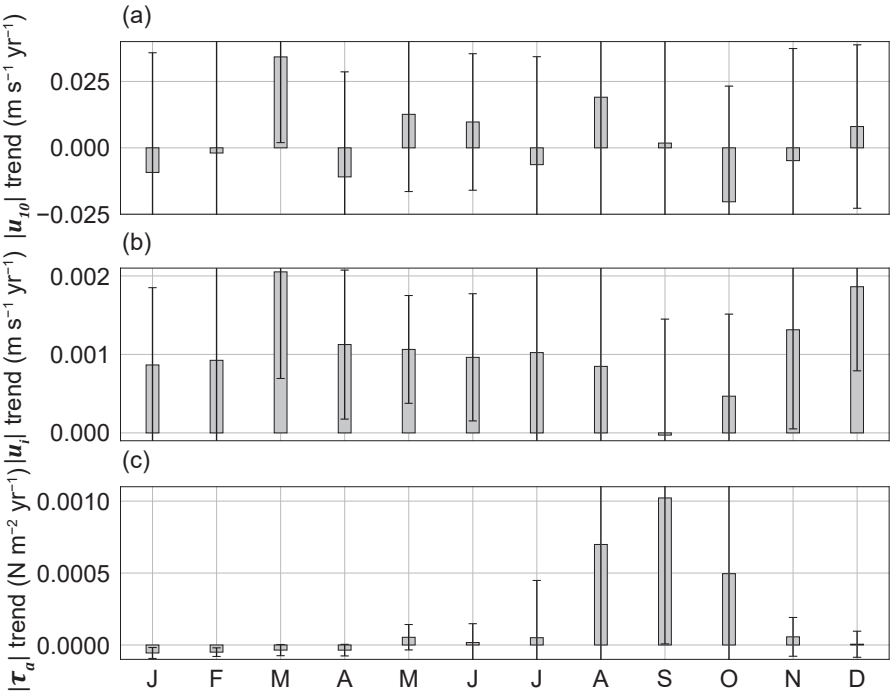

Figure S4. Monthly linear trends of a) mean magnitude of 10 m wind velocity ($|\boldsymbol{u_{10}}|$), b) mean sea-ice drift speed ($|\boldsymbol{u_i}|$, gray), and c) air-ocean stress magnitude ($|\boldsymbol{\tau_a}|$) over the CCB for the 2003–2023 period. Error bars indicate the 95% confidence interval of the linear trend.

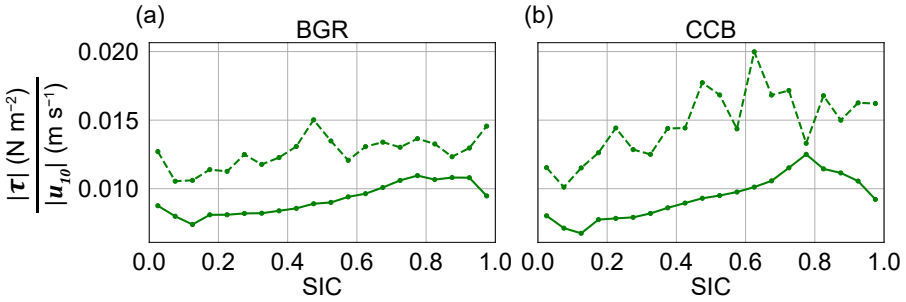

Figure S5. The magnitude of surface stress normalized by wind speed ($\frac{|\boldsymbol{\tau}|}{|\boldsymbol{u_{10}}|}$) as a function of sea-ice concentration (SIC) for all days in September–December (solid green) and during high-stress events (dashed green) for the a) Beaufort Gyre region (BGR) and b) central Canada basin (CCB) over the 2003–2023 period.

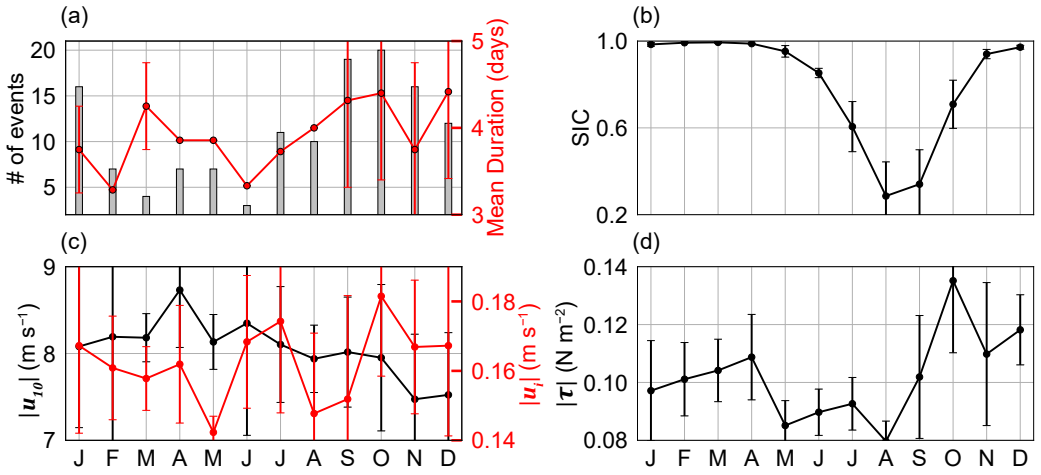

Figure S6. a) Number of high-stress events (gray) and mean duration (red) in the central Canada basin (CCB) by month for 2003–2023. b) Monthly mean sea ice concentration (SIC) during high-stress events in the CCB for 2003–2023. c) Monthly mean wind speed ($|\boldsymbol{u_{10}}|$, black) and mean ice drift speed ($|\boldsymbol{u_i}|$, red) during high-stress events in the CCB for 2003–2023. d) Monthly median magnitude of surface stress ($|\boldsymbol{\tau}|$) during high-stress events in the CCB for 2003–2023. Error bars indicate one median absolute deviation for each month.

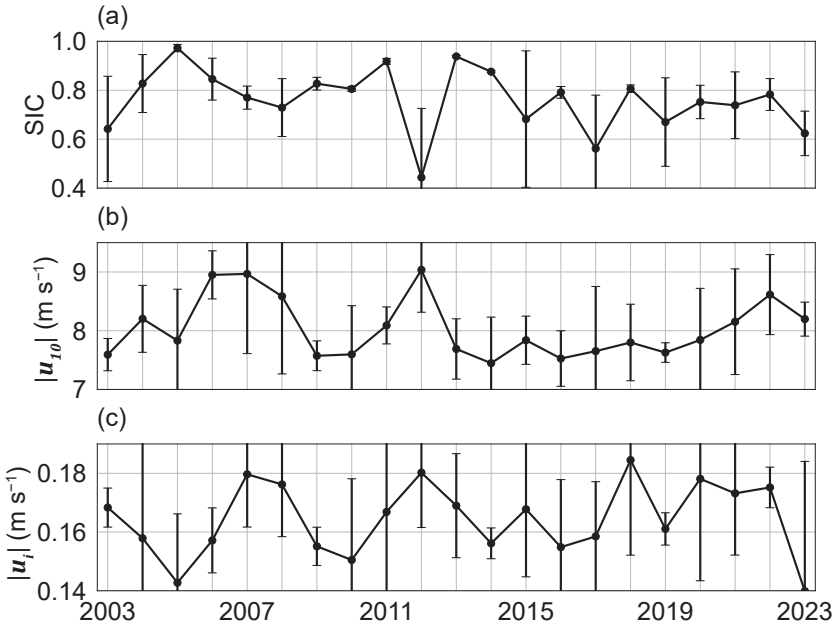

Figure S7. Mean annual a) sea ice concentration (SIC), b) wind speed ($|\boldsymbol{u_{10}}|$), and c) sea-ice drift speed ($|\boldsymbol{u_i}|$) during high-stress events (HSEs) in the CCB for 2003–2023. Error bars indicate one median absolute deviation for each year.

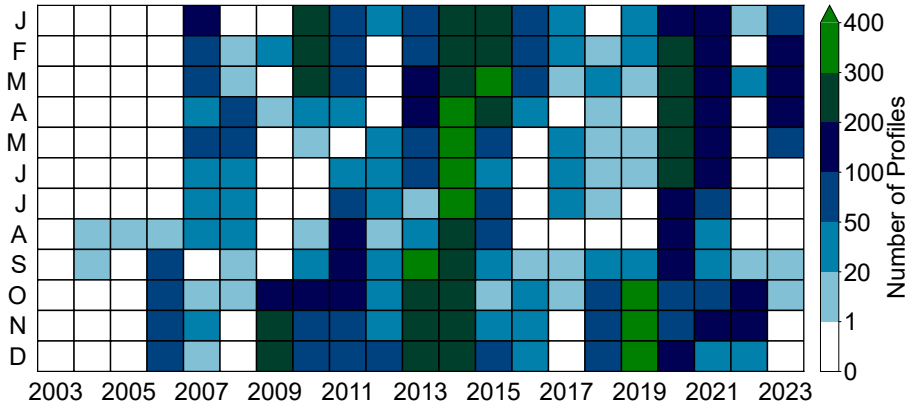

Figure S8. Number of oceanographic profiles per month in the CCB from 2003–2023. Data are from Ice-Tethered Profilers (ITP) and conductivity-temperature-depth (CTD) profiles from BGOS/JOIS cruises.

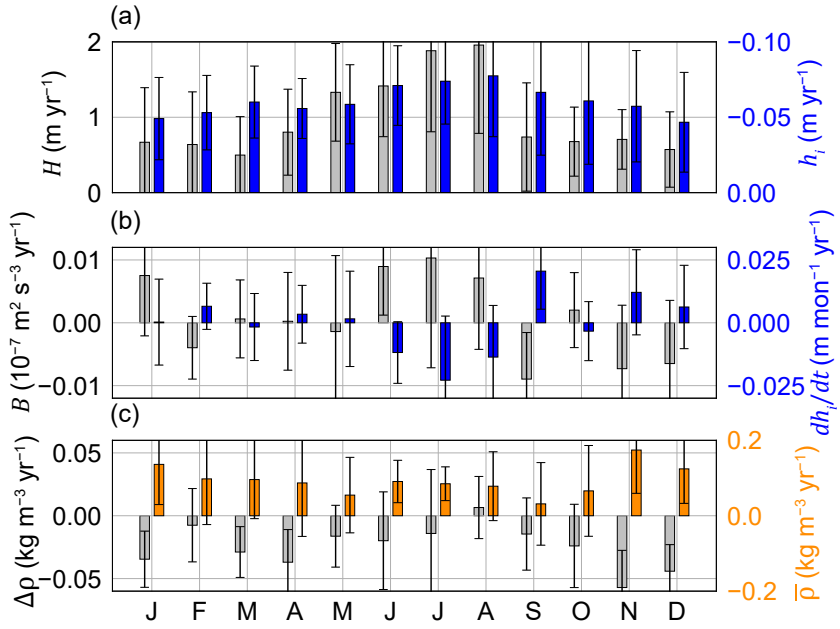

Figure S9. Monthly linear trends of a) mean mixed-layer thickness (H, gray) and sea-ice thickness (h_i, blue), b) mean buoyancy flux (B, gray) and mean monthly sea-ice thickness change ($\frac{dh_i}{dt}$, blue), and c) the density difference across the base of the mixed layer ($\Delta\rho$, gray) and mixed-layer density ($\overline{\rho}$, orange) over the CCB for the 2003–2019 period. Error bars indicate the 95% confidence interval of the linear trend.

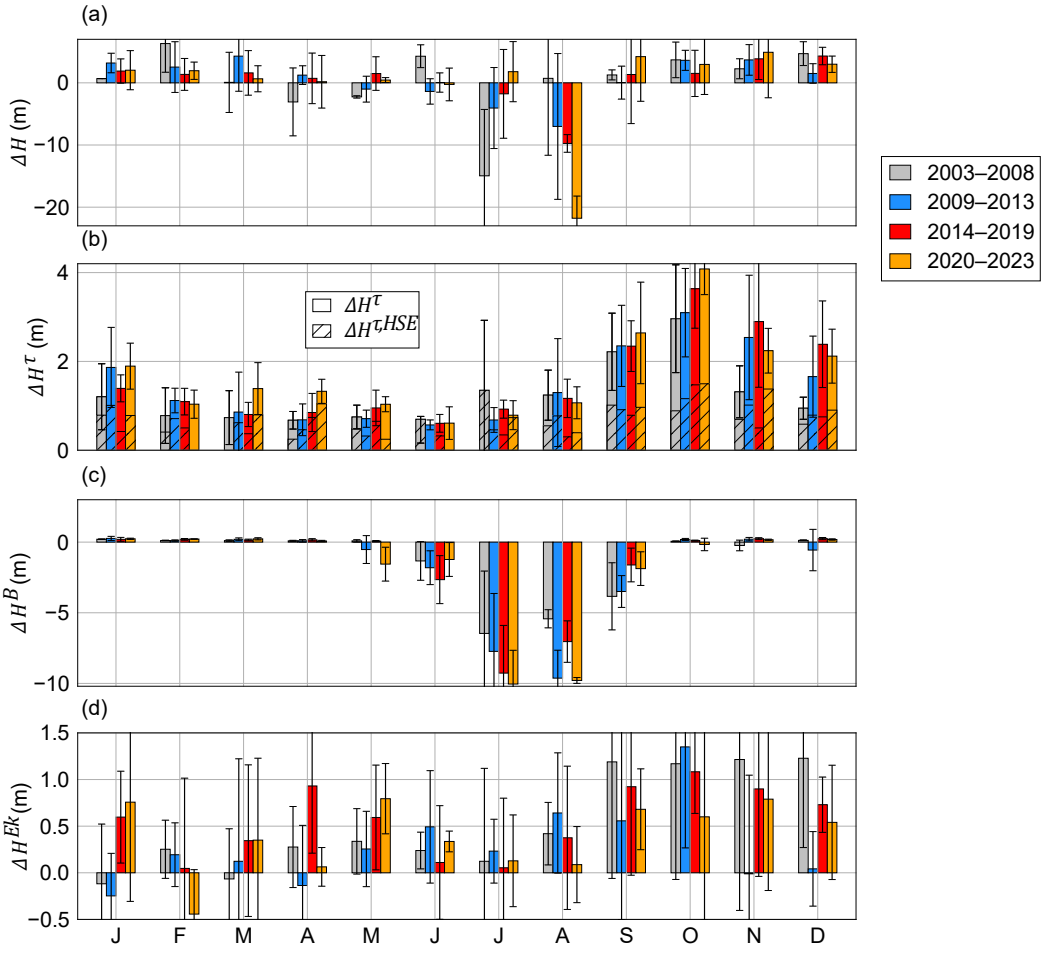

Figure S10. Monthly climatology of total a) observed change in mixed-layer thickness (ΔH), b) stress-induced mixed-layer entrainment (ΔH^{τ}, solid) and mechanical entrainment during High-Stress Events ($\Delta H^{\tau,HSE}$, hatched), c) buoyancy-driven mixed-layer change (ΔH^{B}, blue), and d) Ekman pumping (ΔH^{Ek}, orange) over the CCB for the 2003–2008 (gray), 2009–2013 (blue), 2014–2019 (red), and 2020–2023 (orange) periods. Error bars indicate the interannual standard deviation for each period. The Ekman pumping rate is computed as $w^{Ek} = \frac{\nabla \times \boldsymbol{\tau}}{\rho_0 f}$ (see Margevich et al. for methodology). Total monthly changes are calculated as $\Delta H = \int_{month} w \, dt$ for each rate of mixed-layer change (w).